Clays and Clay Minerals, Vol. 59, No. 6, 595–607, 2011.

HYDRO-MECHANICAL AND CHEMICAL-MINERALOGICAL ANALYSES OF THE BENTONITE BUFFER FROM A FULL-SCALE FIELD EXPERIMENT SIMULATING A HIGH-LEVEL WASTE REPOSITORY

Ann Dueck[1], Lars-Erik Johannesson[1], Ola Kristensson[1,*], Siv Olsson[1], and Anders Sjöland[2]

[1] Clay Technology AB, Ideon Science Park, SE-223 70 Lund, Sweden
[2] Swedish Nuclear Fuel and Waste Management Co., Box 250, SE-10124 Stockholm, Sweden

Abstract—The effect of exposure to repository-like conditions on compacted Wyoming bentonite was determined by comparing the hydraulic, mechanical, and mineralogical properties of samples from the bentonite buffer of the Canister Retrieval Test (CRT) with those of reference material. The CRT, located at the Swedish Äspö Hard Rock Laboratory (HRL), was a full-scale field experiment simulating conditions relevant for the Swedish, so called KBS-3, concept for disposal of high-level radioactive waste in crystalline host rock. The compacted bentonite, surrounding a copper canister equipped with heaters, had been subjected to heating at temperatures up to 95ºC and hydration by natural Na-Ca-Cl type groundwater for almost 5 y at the time of retrieval.

Under the thermal and hydration gradients that prevailed during the test, sulfate in the bentonite was redistributed and accumulated as anhydrite close to the canister. The major change in the exchangeable cation pool was a loss in Mg in the outer parts of the blocks, suggesting replacement of Mg mainly by Ca along with the hydration with groundwater. Close to the Cu canister, small amounts of Cu were incorporated into the bentonite. A reduction of strain at failure was observed in the innermost part of the bentonite buffer, but no influence was noted on the shear strength. No change in swelling pressure was observed, while a modest decrease in hydraulic conductivity was found for the samples with the highest densities. No coupling was found between these changes in the hydro-mechanical properties and the montmorillonite – the X-ray diffraction characteristics, the cation exchange properties, and the average crystal chemistry of the Na-converted <1 μm fractions provided no evidence of any chemical/structural changes in the montmorillonite after the 5 y hydrothermal test.

Key Words—Bentonite, Field Experiment, Hydraulic Conductivity, Hydrothermal, Montmorillonite, High-level Waste, Repository, Swelling Pressure, Unconfined Compression.

INTRODUCTION

In the Swedish so-called KBS-3 concept, designed by the Swedish Nuclear Fuel and Waste Management Co (SKB), for disposal of high-level radioactive waste, spent fuel will be stored in Cu canisters (embedded in a bentonite buffer) which are placed in boreholes at a depth of ~500 m in crystalline bedrock. Required functions of the buffer are to serve as mechanical support for the canister and to act as a barrier to water flow across the deposition hole (SKB, 2006). A buffer of highly compacted bentonite is considered the best choice to fulfill these requirements thanks to favorable hydro-mechanical and chemical properties, such as low hydraulic conductivity, good swelling ability, and plasticity. The long-term performance of the buffer depends heavily on the stability of the bentonite when subjected to the environment expected in a repository, which includes elevated temperatures and hydration by groundwater of variable composition. The most adverse effect on the bentonite properties would probably be the thermally induced conversion of smectite to illite or other non-swelling clay minerals, but other various processes connected to dissolution/precipitation reactions and solute transport may also negatively influence the swelling ability and other hydro-mechanical properties of the buffer. The design criteria for the KBS-3 repository stipulate that the temperature should never exceed 100ºC at any position in the buffer. Karnland and Birgersson (2006), using the kinetic model and constants of Huang *et al.* (1993) and extreme values of the potassium concentration in the groundwater at the Äspö HRL, estimated the smectite-to-illite conversion under these conditions to be insignificant.

During recent decades, a growing number of laboratory and field tests at different scales, designs, and durations were performed in order to study the effects of simulated repository-like conditions on bentonite clays. These experiments mainly highlighted thermo-hydraulic processes, water, and solute transport, and geochemical reactions under the thermal and hydraulic gradients prevalent during the initial stage of the operation of a repository (Karnland *et al.*, 2000; Dixon *et al.*, 2002; ENRESA, 2006; Plötze *et al.* 2007; Villar and Lloret, 2007; Gens *et al.*, 2009; Karnland *et al.*, 2009;

* E-mail address of corresponding author:
Ola.Kristensson@claytech.se
DOI: 10.1346/CCMN.2011.0590605

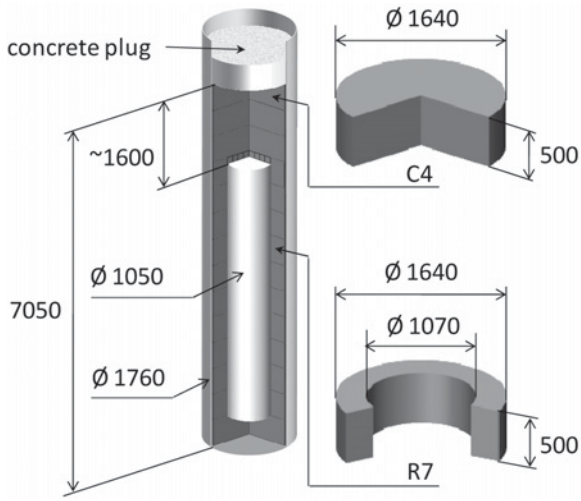

Figure 1. Schematic drawing of the Canister Retrieval Test. ∅ indicates diameter and lengths are given in mm.

Fernández and Villar, 2010; Gómez-Espina and Villar, 2010).

The CRT was a 5 y long, full-scale experiment at Äspö HRL, Sweden, managed by SKB. The layout of the experiment followed the design of the KBS-3 concept (SKB, 2006). The primary aims of the experiment were to demonstrate a technique for retrieving emplaced canisters when the bentonite buffer is completely hydrated (Eng, 2008), and to monitor thermal, hydraulic, and mechanical processes in the bentonite during the operation (Goudarzi and Börgesson, 2006). Moreover, the state of the buffer at excavation was evaluated in terms of water content and dry density (Johannesson, 2007). The CRT experiment also offered opportunities for studying the effects on the bentonite of the exposure to conditions similar to those expected during the initial operational stage of a KBS-3 repository. The results of the studies of the hydro-mechanical and chemical-mineralogical properties of the bentonite at the end of the test are reported here.

THE CRT FIELD EXPERIMENT

In the CRT field experiment, a canister was placed in a deposition hole located in the granitic bedrock at the −420 m level in the Äspö HRL. Essentially, the CRT experiment consisted of a full-size Cu canister, surrounded by ten ring-shaped blocks of compacted bentonite, and cylinder-shaped bentonite blocks placed below and above (Figure 1). The canister was equipped with heaters to simulate the heat generation from spent nuclear fuel. The bentonite blocks were of Wyoming bentonite (Volclay® MX-80 from American Colloid Company), compacted by a tentative method in which a lubricant was applied to the walls of the mould. The compaction pressure when manufacturing the blocks was 40 MPa for the cylinders, which gave a dry density of 1700 kg/m^3, and 100 MPa for the rings, which gave a dry density of 1780 kg/m^3. The initial water content was ~17%, which means that the clay was unsaturated. Thus, a limited amount of air was present in the pores of the bentonite at the time of installation. A 6 cm slot between the bentonite blocks and the borehole wall was filled with bentonite pellets.

The bentonite had been subjected to hydration through filters by a natural Na-Ca-Cl type groundwater (~4000 mg Cl^-/L) and elevated temperature for almost 5 y when it was retrieved in 2006. Sensors were placed in the buffer at selected locations to monitor thermo-hydro-mechanical (THM) processes during the entire experiment. The recorded temperature evolution (Figure 2, left) in the buffer at mid-height of the canister (ring 5) and at the top (cylinder 4) showed that steady-state heat flow conditions were reached during the first year of the experiment. The temperature was maintained at ~95ºC at the canister surface with a radial thermal gradient of ~1ºC/cm for ~2 y (Figure 2, right).

The upper half of the buffer was sampled, while the lower half was used for testing the retrieval technique. The state of the bentonite buffer at the time of excavation, in terms of water content, dry density, and water saturation (Figure 3), was reported by Johannesson

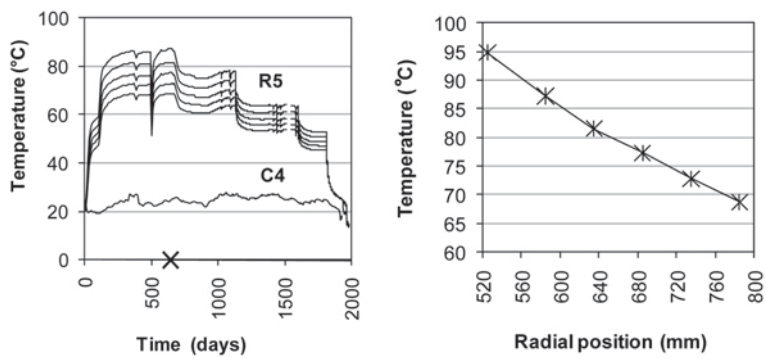

Figure 2. Left: The measured temperature evolution in the buffer at the points indicated (in Ring 5 and Cylinder 4). Right: The temperature profile in the buffer at canister mid-height (in Ring 5) at day 643 (indicated in the left figure). The temperature at 525 mm has been calculated assuming perfect radial heat flow.

(2007). In block R7, approximately at mid-height of the canister, the final state of the buffer (the pellet slot is excluded in the description below) was fully water saturated and had an approximately homogeneous dry density of 1600 kg/m^3. In block C4, above the canister, the buffer had a water saturation of 80% and a dry density of 1650 kg/m^3 in the central parts, and at the parts close to the slot with pellets it was fully water saturated and had a dry density of 1500 kg/m^3.

MATERIAL AND METHODS

Sampling

Samples were taken from two blocks, R7 surrounding the heated canister and C4 which was not in contact with the canister. Unaltered MX-80 bentonite, collected at the time of manufacture of the blocks, was used as the reference material. In general, each field-test sample consisted of 20−50 mm of the block radius. To increase the spatial resolution at the heater, and also to determine specifically the potential effects of the lubrication in connection with the block production, the inner surface of block R7 (sample R7 525) was sampled separately by scraping off a 1−2 mm thick layer, which was analyzed for mineralogy and chemistry.

The samples were labeled with the block number and the radial position, *e.g.* R7 635 indicates that the sample was taken from block R7 at a radial distance of 635 mm from the center of the deposition hole. The corresponding reference sample was labeled R7 R.

Chemical and mineralogical analyses

Sample preparation. The silicate chemistry, the mineralogy, and the cation exchange capacity (CEC) were determined both for bulk samples and the fine clay (<1 μm) fractions. Prior to separation by size, the bentonite was converted to homoionic Na-clay. Excess salt was removed by centrifuge washing, followed by dialysis (Spectrapor® 3, 3500 MWCO dialysis membrane: Spectrum Europe, Breda, The Netherlands) against deionized water until the electrical conductivity of the external water remained at <10 μS/cm for 5 days. After completion of the dialysis, the dispersed sample was centrifuged with a time and speed, calculated by Stokes' Law, to correspond to a particle separation at an equivalent spherical diameter of <1 μm.

Bentonite composition. The chemical composition of the bulk bentonite and of the Na-exchanged <1 μm fraction was determined by inductively coupled plasma atomic emission spectroscopy (ICP-AES) analysis at an ISO 9001 certified laboratory, using standard techniques for silicate analysis (fusion with Li-borates followed by nitric acid digestion). Total carbon and sulfur were determined by evolved gas analysis by combustion of the samples in a Leco furnace. Carbonate carbon was determined as evolved CO_2 on treatment with hot 15% HCl.

Aqueous leachates. Aqueous leaching at a low solid:liquid ratio was used to determine the inventory of soluble salts and solutes (sulfates and chlorides). Dried and ground samples of the bulk bentonite were dispersed in deionized water at a solid:liquid ratio of 1:100 and the suspension was left at room temperature under atmospheric conditions for 5 days to allow equilibration and sedimentation. After phase separation by centrifugation and filtration (0.8 and 0.2 μm syringe filters Acrodisc PF), major anions were determined using ion chromatography.

Cation exchange capacity ($CEC_{Cu\text{-}trien}$) and exchangeable cations. The CEC of the bulk bentonite and of the Na-exchanged <1 μm fraction were determined by exchange with Cu(II)-triethylenetetramine (Cu-trien) following the procedure of Meier and Kahr (1999), modified according to Ammann *et al.* (2005). $CEC_{Cu\text{-}trien}$ was calculated on the basis of the uptake of the Cu(II) complex by the clay. All $CEC_{Cu\text{-}trien}$ determinations were carried out in duplicate.

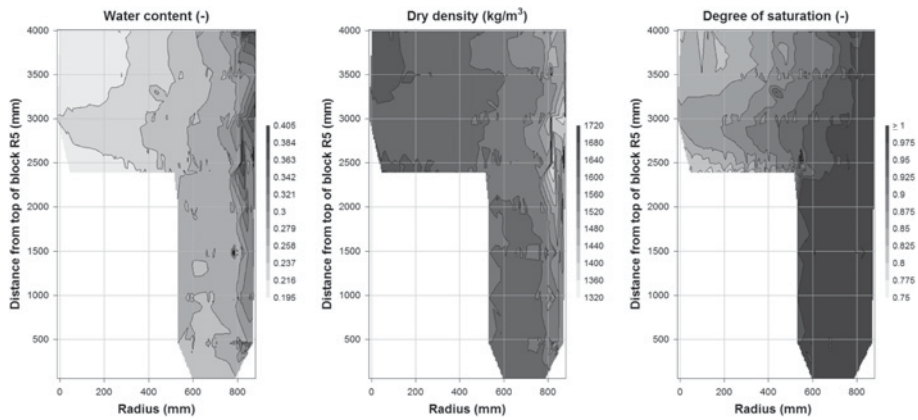

Figure 3. State of the buffer measured after the excavation: water content, w (mass of water/mass of solid), dry density, ρ_d, and degree of saturation, S_r (volume of water/pore volume).

Gypsum and calcite will dissolve in the Cu-trien solution, which makes this extractant unsuitable for determining the exchangeable cations (*e.g.* Dohrmann and Kaufhold, 2010). Therefore, the exchangeable cations of the bulk bentonite were extracted by three successive displacements with ammonium in an alcoholic solution (0.15 M NH_4Cl in 80% ethanol) according to a procedure originally recommended for determining the CEC of gypsiferous/calcareous soils (*e.g.* Belyayeva, 1967; Jackson, 1975). An alcoholic solution was used to minimize dissolution of gypsum and calcite, but chlorides and sulfates/carbonates of alkali metals, if present, will also dissolve in this extractant. Ca, Mg, Cu, Na, and K in the extracts were determined by ICP-AES. The extractions were performed in duplicate for block R7.

The water content of the bentonite was determined for a separate sample dried at 105ºC for 24 h.

X-ray diffraction analysis. The mineralogical composition was determined by X-ray diffraction (XRD) analysis of randomly oriented powders of the bulk material ground to a grain size <10 μm. The <1 μm fraction of the samples from block R7 was converted to Mg-clay and X-ray scanned as oriented mounts in an air-dried state and after ethylene glycol (EG) solvation. A Seifert 3000 TT X-ray diffractometer (Ahrensburg, Germany) with CuKα radiation and automatic slits was used for the XRD. The step size was 0.02º2θ and the scanning speed 1º2θ/min.

Hydro-mechanical analyses

Swelling pressure and hydraulic conductivity tests. The hydraulic conductivity and swelling pressure are essential properties of the buffer material in a repository. These parameters depend heavily on the density of the material, the chemical composition of the water, and the type of buffer material (Börgesson *et al.* 1995; Dixon *et al.* 1999; Karnland *et al.*, 2006, 2008).

The hydraulic conductivity and swelling pressure tests were carried out in test cells (diameter = 50 mm; height of the samples = 20 mm). The specimens were saturated by water infiltration through two filters placed at the bottom and top of the samples (Figure 4, left).

A piston was placed on top of the specimen in order to keep its volume constant and the swelling pressure was measured continuously during saturation with a load cell (Figure 4, left). The specimens were saturated with groundwater from the test site.

Twelve tests were performed on trimmed specimens from blocks C4 and R7. A further six tests were carried out on material taken from the field experiment which was air dried and crushed to a grain size similar to that of MX-80 and compacted into the test cells to dry densities of ~1550 kg/m^3, which, after homogenization of the buffer, corresponded to a density at saturation of ~2000 kg/m^3, *i.e.* the reference density for the KBS-3 concept. In addition, six reference tests were performed on the same bentonite used in the manufacture of the buffer blocks. These specimens were compacted into the test cells to dry densities of between 1310 and 1580 kg/m^3 in order to cover the expected density range in the field experiment.

After saturation, a water-pressure gradient was applied over the specimen and the volume of the outflowing water measured until the flow-rate was stable. The hydraulic conductivity was then calculated according to Darcy′s law. The hydraulic gradient during the tests varied between 3750 and 7500 m/m, corresponding to a pore-pressure difference over the sample, P_w, of 750−1500 kPa. No backpressure was used, *i.e.* the pore pressure at the outlet was atmospheric. The measurements of the outflow were made over several days in order to obtain stable values of the hydraulic conductivity evaluated.

The water content and density were determined for each specimen after testing. The water content was determined as the ratio of the mass of water to the dry mass, where the dry mass was determined after drying at 105ºC for 24 h. The bulk density was calculated from the total mass of a sample and the volume determined by weighing the sample above and submerged in paraffin oil. To determine the degree of saturation, a particle density of 2780 kg/m^3 (Börgesson *et al.* 1995) and water density of 1000 kg/m^3 were used together with the water content determined and bulk density.

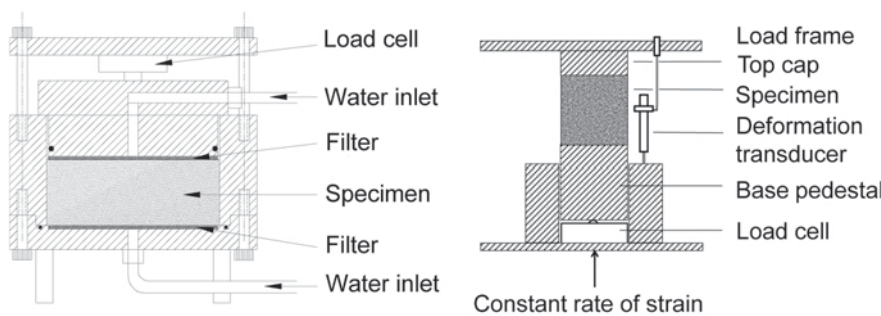

Figure 4. Schematic drawing of a test cell used for determining swelling pressure and hydraulic conductivity (left); the set-up for the unconfined compression test (right).

Unconfined compression tests. The unconfined compression test method was used in several studies by Börgesson *et al.* (2004), Dueck (2010), Dueck *et al.* (2010), and Karnland *et al.* (2009) where the mechanical properties of bentonite were of interest. The unconfined compression test is an experimentally simple method where a cylindrical specimen is compressed axially under a constant rate of strain with no radial confinement or external radial stress.

Two types of specimens were prepared, one tall (40 mm) used for determination of shear strength and one short (20 mm) used for comparison of mechanical behavior between specimens taken from different positions and reference specimens. The shear strength is commonly determined on specimens with a height equal to double the size of the diameter to allow the shear failure to develop fully without boundary effects from the end surfaces. The second type of specimens had height equal to the diameter of the specimen, and the end effect was minimized by lubrication of the end surfaces. The diameter of the specimens was kept at 20 mm in order to optimize the spatial resolution across the profile of the field experiment.

Samples were taken from different positions along the radius of blocks R7 and C4. A total of 35 drilled samples and 13 reference specimens of the short variety were tested, while six drilled samples and four reference specimens of the tall variety were tested. The samples from the field experiment were prepared by drilling and trimming cylindrical specimens, 20 mm in diameter and 20 mm tall. The reference specimens of the same dimensions were prepared from powder in a compaction device.

All specimens were saturated in a device, using the same technique as described in the section 'Swelling pressure and hydraulic conductivity tests.' The saturation began after evacuation of air from the filters and tubes and was performed over a period of 2 weeks, using groundwater from the test site. The specimens were removed from the saturation device at least 12 h before the shearing tests. In order to reduce the saturation time for the tall specimens, two short specimens were used and placed on top of each other.

The specimens were placed in a mechanical press (Figure 4, right) and the compression was run at a constant strain rate of 0.8%/min which corresponds to 0.16 mm/min for the short specimens and 0.32 mm/min for the tall specimens. During compression, the specimens were surrounded by a thin plastic film to minimize evaporation of water. After failure the water content and density were measured in the same way as for the swelling pressure and hydraulic conductivity tests.

RESULTS AND DISCUSSION

Chemical and mineralogical analyses

Aqueous leachates. The inventory of soluble chlorides and sulfates in the bentonite retrieved and in the reference samples was compared quantitatively with the chloride and sulfate concentrations in the groundwater at Äspö by recalculating the contents determined as mg/g of dry bentonite as molar concentrations by use of the water content of the samples (Figure 5).

The central part of block C4 was not fully water saturated at the retrieval (*cf.* Figure 3), which was reflected as a steep gradient in the chloride concentration toward the center of the block, where the concentration remained the same as that of the reference bentonite. In the fully saturated block R7, the hydration by groundwater resulted in an increased and constant concentration of chloride. The chloride concentration was, however, still lower than that of the Äspö groundwater, which is qualitatively consistent with ion equilibrium theory, predicting a lower anion concentration in the interlayers of the smectite than in the external groundwater, due to the equilibrium demand of equal activity products (Birgersson and Karnland, 2009).

The sulfate concentration in the water extracts of the MX-80 reference samples was much higher than that of the Äspö groundwater, proving that the inventory of gypsum in the MX-80 bentonite was the main source of sulfate. The concentration in block C4 was more or less constant and the same as that of the reference bentonite. In contrast, the heated block R7 displayed a sulfate maximum near the canister, and XRD analysis confirmed that anhydrite ($CaSO_4$) had formed there. The

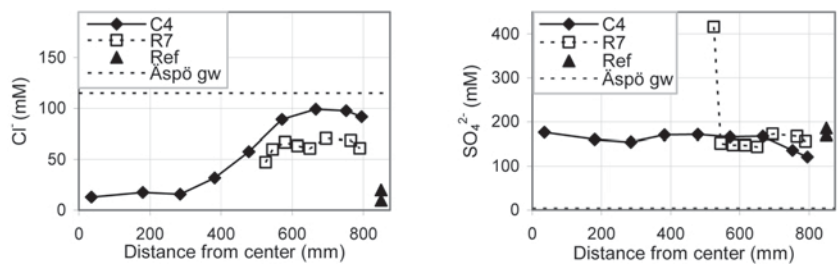

Figure 5. The radial distribution of Cl^- and SO_4^{2-} in water extracts of bulk samples from blocks C4 and R7. The concentration of the reference samples is shown at position 850 mm. The dotted line shows the mean concentrations in the ground water at Äspö during the period 1999–2004.

behavior of calcium sulfates, which have temperature-dependent solubility, was clearly influenced by the non-isothermal conditions and the hydration gradients that prevailed in the heated part of the buffer. The results agreed with those reported for a field test with the same design and components as the CRT experiment but of smaller scale and with steeper temperature gradient (Karnland *et al.* 2009), and also with results of laboratory experiments with compacted Ca-Mg bentonite heated at 100ºC (Fernández and Villar, 2010). In both cases gypsum/sulfate was observed to leach from the bentonite in the proximity of the hydration source and that calcium sulfate accumulated in the heated part.

Bentonite composition. The sulfate and carbonate minerals are trace constituents in MX-80, but attention was paid to these minerals because of their temperature-dependent solubility, which affects behavior under non-isothermal conditions. The acid-soluble carbon content, derived mainly from carbonate phases ($C-CO_3$ in Table 1), was 0.12−0.13% C (detection limit 0.02%) in the reference bentonites. The concentration in the block samples remained in the same range after the hydrothermal exposure, with no discernible trends in any of the blocks.

The total sulfur content in the reference bentonites was 0.27−0.28% (detection limit 0.02%), with 40−50% originating from gypsum. In the blocks retrieved, the distribution of total sulfur was consistent with the results of the aqueous leaching, indicating sulfate accumulation near the heater in block R7.

The chemical data for the bentonite (Table 1) further showed that Cu was incorporated in the bentonite adjacent to the Cu canister (sample R7 525). Despite prolonged washing/dialysis in the purification procedure, the <1 μm fraction had a slightly larger Cu content (497 mg/kg) than the bulk bentonite (414 mg/kg; Table 1), but treatment of a sub-sample of the clay with an acetic acid-sodium acetate buffer at pH 5 extracted much of the Cu. The dissolution behavior indicated that Cu was not a structural element in the smectite, but fixed in the clay in a water-insoluble form, possibly as adsorbed complexes or precipitates. Using optical and electron microscopy combined with thermal analysis, Kaufhold and Dohrmann (2007) identified a Cu-S phase as the major product of Cu corrosion in a study of the bentonite from the LOT field test, which had similar design to the CRT experiment.

The redox conditions in the buffer were not monitored during the field test, but corrosion of the Cu canister may be explained by reactions during an early stage of the test when oxygen existed in the system, trapped in pores and dissolved in water.

The samples of the inner surface of block R7 contained conspicuously large amounts of organic carbon and levels of Mo, P, and Zn that were significantly greater than the normal concentration range in MX-80 (Table 1). This combination of elements clearly suggested adsorption of the lubricant used in the block production, which contained distillates of mineral oil with Mo-, Zn-, and P-bearing additives.

Exchangeable cations and $CEC_{Cu\text{-}trien}$. In general, a reasonably good match was found between the sum of the exchangeable cations, extracted into alcoholic ammonium chloride solution, and the $CEC_{Cu\text{-}trien}$ of the samples, indicating that dissolution of salts during the extraction into alcoholic solution contributed little to the extracted cation population (Table 2).

The proportions between the major exchangeable cations, Na, Ca, Mg, and K, in the block samples were essentially the same as in the reference samples, *i.e.* about two thirds of the exchange sites were occupied by Na and Ca was second most abundant. The most obvious tendency was an overall depletion in Mg, relative to the reference samples, in the outer parts of both blocks at the borehole wall, suggesting some replacement of exchangeable Mg, mainly by Ca, during the hydration with the Na-Ca dominated groundwater.

The Cu concentrations in clear excess of the analytical detection limit were found only in the extract of sample R7 525.The amount of exchangeable Cu was <<1% of the total exchangeable cation pool and made up <8% of the maximum available amount of Cu, 414 mg/kg (Table 1), which suggested that Cu in the bentonite was not readily accessible for cation exchange.

The $CEC_{Cu\text{-}trien}$ of the reference bentonites, 81−82 meq/100 g, matched the $CEC_{Cu\text{-}trien}$ value previously reported for the bentonite MX-80 (*e.g.* Karnland *et al.*, 2009). No significant difference could be seen among the block samples, and those small variations that existed appeared to be random and independent of the position of the sample in the blocks. The same was true for the $CEC_{Cu\text{-}trien}$ of the <1 μm fractions. Somewhat smaller $CEC_{Cu\text{-}trien}$ values (values within parentheses in Table 2) were obtained for the 1−2 mm thick layer scraped off the inner surface of block R7 (sample R7 525), the chemical composition of which clearly suggested contamination by the lubricant used in the block production. Therefore, the CEC values were considered uncertain, both because of the dilution effect (~2.5% organic C) and because the contaminant itself may give rise to artifacts in the CEC determination.

Montmorillonite composition. The chemical data for the Na-exchanged <1 μm fraction (Table 1) were used for calculations of the structural formula of the smectite with the following assumptions and simplifications: (1) all structural Fe was assumed to be trivalent although no determination was made of the oxidation state. The assumption that all octahedral Fe was present only in the ferric state may underestimate the octahedral charge. (2) Ca was assigned to the pool of interlayer cations because any calcium carbonate/sulfate that survived the

Table 1. Chemical composition of the bulk samples (b) and the Na-exchanged <1 μm fractions (c) from block C4, R7, and reference samples.

Sample		SiO_2 (%)	Al_2O_3 (%)	Fe_2O_3 (%)	MgO (%)	CaO (%)	Na_2O (%)	K_2O (%)	TiO_2 (%)	P_2O_5 (%)	MnO (%)	Mo (%)	Ba (mg/kg)	Cu (mg/kg)	Zn (mg/kg)	LOI (%)	Sum (%)	Tot C (%)	Tot S (%)	$C-CO_3$ (%)
C4 035	b	62.8	19.96	3.55	2.49	1.18	2.17	0.54	0.14	0.04	0.01	<.001	425	5	69	7.0	100.07	0.26	0.28	0.14
	c	63.7	20.55	3.75	2.54	0.11	2.39	0.08	0.10	0.03	0.01	<.001	29	<5	34	6.5	99.84	0.15	0.02	n.d.
C4 180	b	62.5	19.83	3.54	2.49	1.12	2.08	0.49	0.14	0.03	0.01	<.001	262	10	51	7.6	99.93	0.26	0.27	0.13
	c	63.6	20.77	3.79	2.63	0.11	2.46	0.07	0.10	0.02	<.01	<.001	24	<5	41	6.4	99.99	0.13	0.02	n.d.
C4 285	b	62.7	19.87	3.54	2.53	1.17	2.07	0.50	0.14	0.06	0.01	<.001	289	5	93	7.2	99.94	0.30	0.27	0.10
	c	63.5	21.09	3.74	2.62	0.10	2.48	0.07	0.10	0.03	<.01	<.001	23	5	33	6.1	99.85	0.14	0.01	n.d.
C4 382	b	61.9	19.69	3.44	2.44	1.19	2.11	0.52	0.14	0.05	0.01	<.001	547	5	88	8.4	100.06	0.28	0.29	0.10
	c	63.2	21.26	3.77	2.63	0.10	2.46	0.07	0.10	0.03	0.01	<.001	22	<5	33	6.3	99.99	0.13	0.02	n.d.
C4 478	b	62.9	19.90	3.63	2.47	1.22	2.12	0.52	0.14	0.05	0.01	<.001	306	5	125	7.0	100.07	0.27	0.29	0.12
	c	63.4	21.15	3.69	2.65	0.11	2.51	0.07	0.10	0.02	0.01	<.001	23	<5	31	6.2	99.98	0.15	0.02	n.d.
C4 571	b	63.2	19.80	3.54	2.49	1.20	2.14	0.53	0.14	0.03	0.01	<.001	321	5	95	6.9	100.06	0.28	0.27	0.10
	c	63.8	20.95	3.81	2.65	0.12	2.44	0.07	0.10	0.03	0.01	<.001	25	<5	32	6.0	99.98	0.14	0.02	n.d.
C4 666	b	63.0	19.98	3.57	2.49	1.15	2.15	0.51	0.14	0.04	0.01	<.001	292	5	59	6.9	100.06	0.28	0.32	0.13
	c	63.0	21.29	3.77	2.64	0.10	2.48	0.07	0.10	0.02	0.01	<.001	22	<5	32	6.5	99.98	0.13	0.01	n.d.
C4 752	b	62.8	20.01	3.64	2.45	1.25	2.17	0.54	0.14	0.05	0.01	<.001	299	5	59	6.9	100.06	0.27	0.27	0.13
	c	63.4	20.93	3.75	2.59	0.11	2.40	0.06	0.09	0.02	0.01	<.001	21	<5	30	6.6	99.99	0.14	0.02	n.d.
C4 795	b	62.4	20.23	3.52	2.47	1.31	2.24	0.54	0.14	0.05	0.01	<.001	262	5	91	7.0	100.06	0.28	0.28	0.11
	c	63.8	20.82	3.80	2.62	0.10	2.50	0.06	0.10	0.02	0.01	<.001	19	<5	24	6.1	99.99	0.12	0.01	n.d.
C4 Ref	b	62.8	20.29	3.64	2.53	1.20	2.20	0.53	0.14	0.04	0.01	<.001	282	5	71	6.6	100.06	0.29	0.27	0.13
	c	63.8	21.01	3.74	2.58	0.10	2.60	0.06	0.10	0.03	<.01	<.001	23	8	27	5.9	99.99	0.19	0.02	n.d.
R7 525	b	60.8	19.09	3.43	2.47	1.74	2.07	0.49	0.14	0.07	0.01	0.018	258	414	374	9.4	99.94	2.51	0.56	0.10
	c	61.5	20.47	3.75	2.52	0.07	2.41	0.07	0.09	0.02	0.01	0.004	14	497	352	8.8	99.85	2.60	0.03	n.d.
R7 545	b	62.8	20.13	3.55	2.51	1.19	2.20	0.55	0.15	0.06	0.01	<.001	344	5	85	6.8	100.07	0.39	0.31	0.10
	c	63.4	20.76	3.88	2.62	0.11	2.46	0.08	0.10	0.02	0.01	<.001	27	12	85	6.5	99.99	0.27	0.01	n.d.
R7 580	b	62.7	20.14	3.58	2.48	1.21	2.23	0.59	0.14	0.05	0.01	<.001	360	9	71	6.8	100.07	0.29	0.28	0.11
	c	63.3	20.93	3.86	2.62	0.10	2.52	0.07	0.10	0.02	0.01	<.001	24	<5	38	6.4	99.98	0.13	0.01	n.d.
R7 615	b	62.6	20.10	3.58	2.45	1.22	2.22	0.56	0.15	0.06	0.01	<.001	321	5	151	7.0	100.07	0.28	0.29	0.12
	c	63.3	20.97	3.82	2.61	0.13	2.47	0.08	0.10	0.03	0.01	<.001	28	<5	31	6.4	99.98	0.15	0.02	n.d.
R7 650	b	62.7	20.03	3.65	2.46	1.18	2.21	0.55	0.14	0.05	0.01	<.001	465	5	75	6.9	100.05	0.28	0.31	0.13
	c	63.8	20.68	3.84	2.61	0.11	2.49	0.08	0.10	0.02	0.01	<.001	28	<5	29	6.2	100.00	0.14	0.02	n.d.
R7 695	b	62.6	19.87	3.60	2.46	1.31	2.14	0.53	0.14	0.04	0.01	<.001	300	5	73	7.1	99.93	0.28	0.30	0.14
	c	63.3	21.02	3.91	2.61	0.12	2.53	0.07	0.10	0.02	0.01	<.001	32	<5	32	6.2	99.98	0.16	0.02	n.d.
R7 765	b	62.2	20.14	3.53	2.48	1.25	2.21	0.55	0.14	0.06	0.01	<.001	365	5	87	7.4	100.06	0.27	0.29	0.14
	c	63.1	20.89	3.83	2.6	0.10	2.57	0.06	0.10	0.04	0.01	<.001	21	<5	30	6.6	99.98	0.15	0.02	n.d.
R7 790	b	62.6	20.29	3.57	2.47	1.25	2.25	0.56	0.15	0.04	0.01	<.001	287	5	86	6.8	100.07	0.28	0.29	0.12
	c	63.5	20.94	3.79	2.52	0.12	2.49	0.09	0.10	0.02	0.01	<.001	31	<5	30	6.4	99.99	0.17	0.02	n.d.
R7 Ref	b	62.3	20.44	3.53	2.52	1.24	2.17	0.56	0.14	0.05	0.01	<.001	294	5	102	7.0	100.07	0.29	0.28	0.12
	c	63.7	20.79	3.79	2.52	0.09	2.56	0.07	0.10	0.03	<.01	<.001	25	<5	28	6.3	99.99	0.15	0.01	n.d.

n.d. = not determined

Table 2. Exchangeable cations (meq/100 g) and CEC of the samples from blocks C4 and R7, and the reference samples for the blocks. CEC values are the mean of two determinations. Values within parentheses are discussed in the text.

	Exchangeable cations						CEC	
Sample	Ca	Cu	K	Mg	Na	Σ	bulk	<1 μm
C4 035	16	0.00	1.3	4.4	56	78	79	93
C4 180	16	0.00	1.4	4.4	55	77	82	92
C4 285	17	0.01	1.4	4.8	54	77	81	93
C4 382	17	0.00	1.4	5.1	54	78	82	93
C4 478	18	0.00	1.4	5.3	55	79	81	92
C4 571	18	0.00	1.4	5.2	55	80	80	91
C4 666	17	0.00	1.5	5.2	55	79	81	92
C4 752	19	0.00	1.7	4.6	56	81	82	93
C4 795	18	0.00	1.5	2.9	55	77	80	92
C4 R	18	0.00	1.6	7.2	54	81	82	92
R7 525	19	0.11	1.5	7.5	53	81	(79)	(91)
R7 545	18	0.00	1.6	6.0	56	81	81	94
R7 580	18	0.00	1.6	5.8	56	81	80	95
R7 615	18	0.01	1.4	5.3	53	77	81	94
R7 650	18	0.00	1.6	5.7	55	81	81	92
R7 695	18	0.00	1.4	5.5	55	79	80	94
R7 765	18	0.00	1.4	4.8	53	77	80	93
R7 790	18	0.00	1.4	4.2	54	78	81	92
R7 R	17	0.00	1.5	6.9	54	80	81	92

sample pre-treatments will dissolve during the dialysis, supplying Ca for exchange. The same would be true for Mg but no soluble Mg-bearing phases were identified. (3) Mg was assigned to the octahedral sheet as the clay was saturated with Na prior to chemical analysis in order to make the allocation of cations to exchange and structural sites, respectively, less ambiguous. Allocation of too much Mg to octahedral sites would underestimate the calculated interlayer charge. (4) All K (range of 0.06−0.09% K_2O) was allocated to illitic layers in the smectite structure as no discrete K-bearing minerals were detectable in any of the XRD profiles of the <1 μm fractions. The proportion was calculated assuming the average K_2O content of illite to be 8.5% and the SiO_2 and Al_2O_3 contents were adjusted accordingly. (5) The remaining silica was allocated to the tetrahedral sheet of the smectite. The XRD profiles of the oriented mounts of the <1 μm fractions (Figure 7 left) suggested, however, that traces of cristobalite may still exist in the purified fine-clay fractions. Remnants of free silica in the smectite will necessarily result in underestimation of the tetrahedral charge. (6) Cu in the contact sample R7 525 was not considered a structural element.

No clear trends were seen in the average crystal chemistry (Table 3), either within or between the blocks, and those variations that existed were within the accuracy of the method.

XRD analyses. The XRD profiles of random powders of the cool block C4 displayed no significant mineralogical changes, either with respect to the type or to the peak intensities of accessory minerals. A variation of the intensity of the feldspar peaks was seen among the samples, but both the excellent {010} and {001} cleavages of feldspars, which promote preferred orientation, and the coarse grain size of feldspars may give rise to a random variation in the peak intensities.

The most conspicuous mineralogical change in the heated block was the appearance of peaks of anhydrite in the sample from the inner surface of the block (Figure 6). Accordingly, the mineralogical data matched the chemical data, which suggested that calcium sulfate had concentrated near the canister surface.

The 060 reflection in the region 60−64°2θ was useful for recognizing changes in the *b* cell dimension of the clay minerals, which would be an expected effect of a change of the cations or the site occupancy in the octahedral sheet, or of the amount of Al in tetrahedral coordination. The position of the 060 peak (Figure 6) was more or less identical in all samples and the indicated *d* value, 0.149−0.150 nm (62°2θ), was in the range typical of the dioctahedral sub-group of smectites, to which montmorillonite belongs.

The XRD profiles of oriented mounts of the fine clay (Figure 7) indicated that all the <1 μm fractions were more or less pure montmorillonite. A weak reflection with a *d* value of 0.405 nm in the XRD profile of the air-dried samples indicated, however, that traces of cristobalite may exist. The homoionic Mg-smectite had a basal spacing of 1.46−1.50 nm when air dried and it expanded to 1.68−1.70 nm upon EG solvation. The series of basal reflections of the expanded clay deviated very little from a complete, periodic diffraction pattern, indicative of well ordered stacking sequences with virtually no interstratification. The content of non-exchangeable K of the <1 μm fraction (0.06−0.09% K_2O) suggested that

Table 3. Calculated structural formula of the smectite in samples from blocks C4 and R7.

	C4 035	C4 180	C4 285	C4 382	C4 478	C4 666	C4 752	C4 795	C4 R
Si	8.00	8.00	7.98	7.95	7.97	7.94	7.99	8.00	7.99
Al	0.00	0.00	0.02	0.05	0.03	0.06	0.01	0.00	0.01
Σtet	8.00	8.00	8.00	8.00	8.00	8.00	8.00	8.00	8.00
Al	3.10	3.08	3.10	3.11	3.11	3.11	3.11	3.08	3.10
Ti	0.01	0.01	0.01	0.01	0.01	0.01	0.01	0.01	0.01
Fe^{3+}	0.36	0.36	0.35	0.36	0.35	0.36	0.35	0.36	0.35
Mg	0.48	0.49	0.49	0.49	0.49	0.49	0.48	0.49	0.48
Σoct	3.95	3.94	3.95	3.97	3.96	3.97	3.95	3.94	3.94
Ca	0.02	0.01	0.01	0.01	0.01	0.01	0.01	0.01	0.01
Na	0.60	0.61	0.61	0.60	0.62	0.61	0.59	0.61	0.64
Σinterlayer	0.64	0.64	0.64	0.63	0.64	0.63	0.62	0.63	0.66
	R7 525	R7 545	R7 580	R7 615	R7 650	R7 695	R7 765	R7 790	R7 R
Si	7.97	8.00	7.98	7.98	7.99	7.97	7.98	7.99	8.00
Al	0.03	0.00	0.02	0.02	0.01	0.03	0.02	0.01	0.00
Σtet	8.00	8.00	8.00	8.00	8.00	8.00	8.00	8.00	8.00
Al	3.10	3.08	3.09	3.09	3.09	3.09	3.09	3.10	3.10
Ti	0.01	0.01	0.01	0.01	0.01	0.01	0.01	0.01	0.01
Fe^{3+}	0.36	0.37	0.36	0.36	0.36	0.37	0.36	0.36	0.36
Mg	0.48	0.49	0.49	0.49	0.48	0.49	0.49	0.47	0.47
Σoct	3.96	3.95	3.95	3.95	3.94	3.95	3.95	3.94	3.93
Ca	0.01	0.02	0.01	0.02	0.02	0.02	0.01	0.02	0.01
Na	0.61	0.61	0.62	0.61	0.62	0.62	0.63	0.61	0.63
Σinterlayer	0.63	0.65	0.64	0.65	0.66	0.65	0.65	0.65	0.65

Calculations are based on the chemical data for the Na-exchanged <1 μm fractions in Table 1.

some illitic layers may exist in the smectite of all samples but in proportions (~1%) too small for detection by use of routine XRD analyses. Thus, the XRD characteristics provided no evidence of any significant structural change of the montmorillonite in any of the samples.

Hydro-mechanical analyses

Swelling pressure and hydraulic conductivity tests. The results of the measurements of the swelling pressure and hydraulic conductivity were plotted as a function of dry density together with the best-fit curve determined for the reference specimens (Figure 8). The dry density was

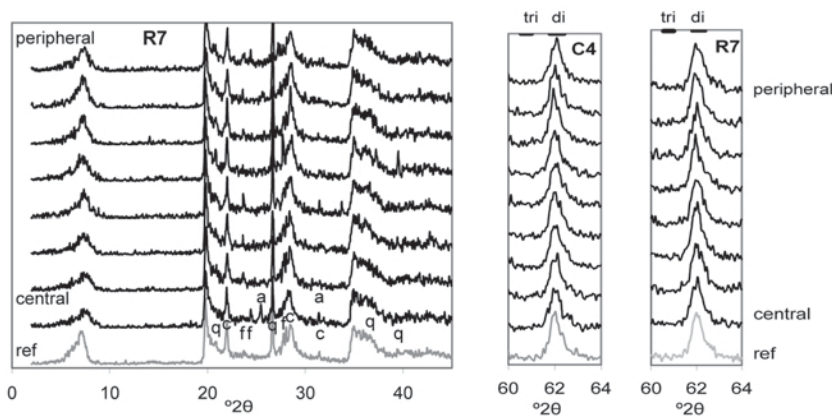

Figure 6. Left: XRD profiles of random powders of bulk samples from block R7 (black curves). Gray curve: mean XRD profile of the reference samples. The position of the strongest peaks of the major non-clay minerals is indicated; a = anhydrite, c = cristobalite, f = feldspars, q = quartz. Right: Close-up of the 060 peak. Black curves: XRD profiles of samples from blocks C4 and R7. Gray curve: mean XRD profile of the reference samples. The positions of the 060 peak of dioctahedral and trioctahedral smectites are indicated on the upper scale. CuKα radiation.

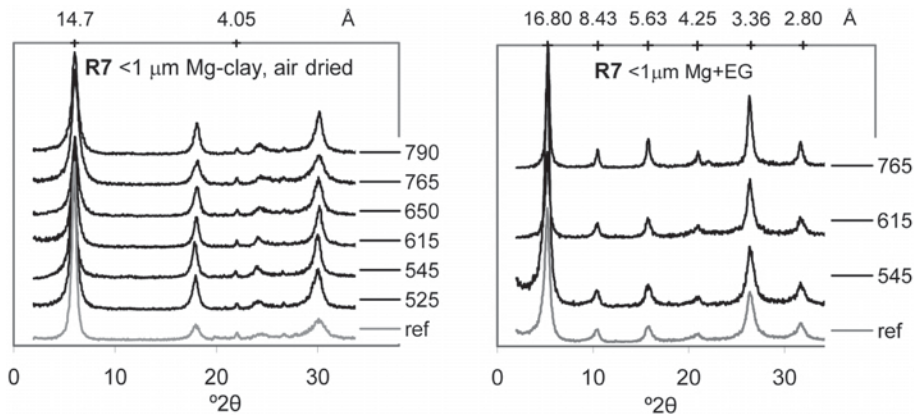

Figure 7. XRD profiles of oriented mounts of the Mg-saturated, air-dried (left) and EG-solvated (right) <1 μm fraction of samples of block R7 (black curves). Gray curve: XRD profile of the reference sample. The position of the basal reflections of montmorillonite is indicated on the upper scale. CuKα radiation.

calculated from the water content and the density measured at the end of the testing following rapid dismantling of the test cell. All tests were performed on water-saturated specimens (S_r > 99%).

The measured swelling pressure and hydraulic conductivity of the field test material were in the same range as the reference material (Figure 8). The data for the air-dried and crushed samples had a significant scatter, compared to the rest of the data set, especially regarding hydraulic conductivity. An analysis of the data showed that the hydraulic conductivity was uncorrelated to the radial distance from the canister, *i.e.* to the maximum temperature during the operation. The scatter might be caused by differences introduced in the preparation process.

The hydraulic conductivity was somewhat lower for the trimmed field test material compared to that of the reference material. This effect was more pronounced at higher densities.

An attempt to evaluate the dependence of hydraulic conductivity on dry density and maximum temperature was performed for the samples from block R7 (Figure 9). Due to the limited amount of data, the analysis was intended to indicate only qualitative properties of the relationships. Three samples were identified as being at 'constant temperature,' in the range 85−87ºC (Figure 9, left; the data points along the arrow parallel to the horizontal axis), and three samples as being at 'constant density,' in the range 1589−1591 kg/m^3 (Figure 9, left; the data points along the arrow parallel to the vertical axis). Straight lines fitted against the 'constant temperature' and 'constant density' samples in the planes of dry density-hydraulic conductivity and temperature-hydraulic conductivity, respectively, indicated the strength of the dependence (Figure 9, middle and right). This analysis showed an insignificant dependence on temperature and the expected significant dependence on dry density.

The findings of the CRT experiment concerning the swelling pressures and hydraulic conductivities agreed with those reported for a field test with similar design but of smaller scale, higher temperature, and steeper temperature gradient (Karnland *et al.* 2009).

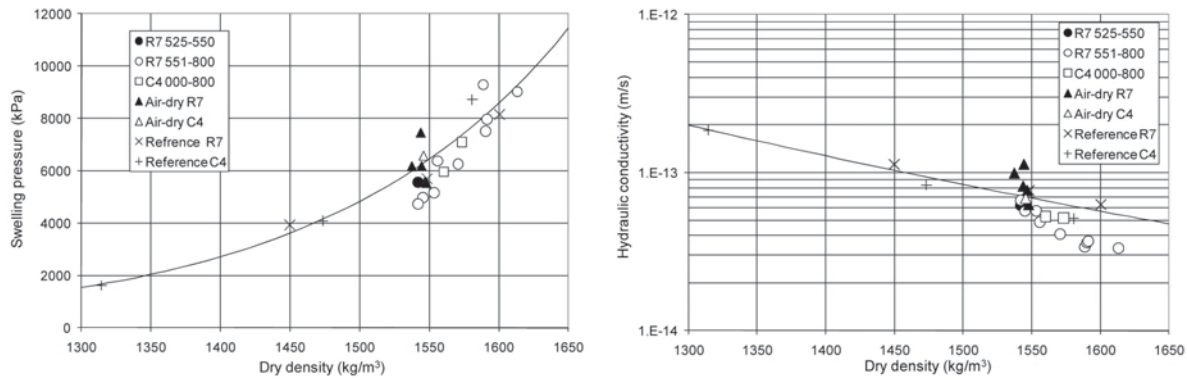

Figure 8. Swelling pressure (left) and hydraulic conductivity (right) plotted as function of the dry density of the samples. The tests were carried out on samples taken from blocks R7 and C4 at different radius from the center of the deposition hole (0−800 mm) and on reference material. The field test material was tested both as trimmed samples and as air-dried, ground, and recompacted samples.

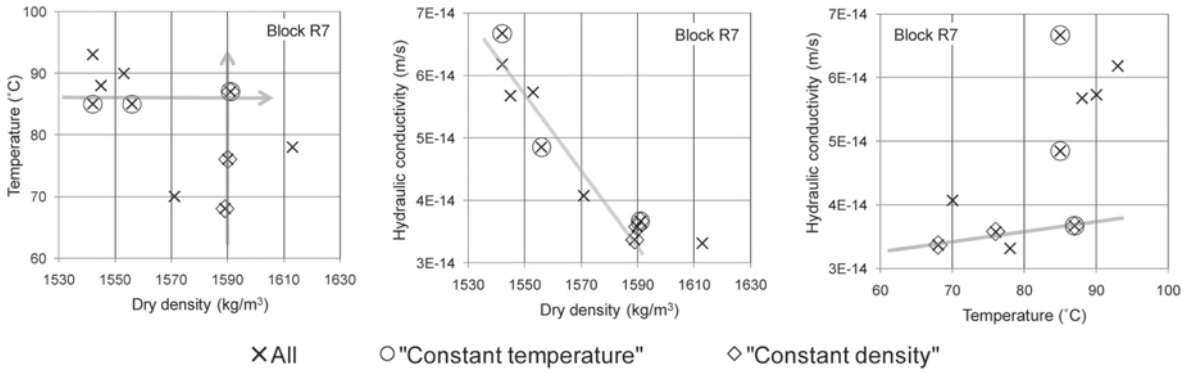

Figure 9. Graphical representations of dry density, maximum temperature, and hydraulic conductivity for samples from block R7. Temperature *vs*. dry density (left). Hydraulic conductivity *vs*. dry density (middle), where the line approximates the dry density dependence. Hydraulic conductivity *vs*. temperature (right), where the line approximates the temperature dependence.

Unconfined compression tests. The specimens were considered as undrained during shearing and no volume change was taken into account. The deviator stress, q (kPa), and the strain, ε (%), were derived from equations 1 and 2, respectively, and calculated from the applied vertical load, F, the original cross sectional area, A_0, the initial length, l_0, and the change in length, Δl. All tests were performed on water-saturated specimens ($S_r \geqslant 99\%$ except for three of the short specimens which had $S_r = 98\%$).

$$q = \frac{F}{A_0}\left(\frac{l_0 - \Delta l}{l_o}\right) \quad (1)$$

$$\varepsilon = \frac{\Delta l}{l_0} \quad (2)$$

The maximum deviator stress, q_{max}, and the corresponding strain, ε, of the material from the field experiment determined on short specimens were plotted with best-fit lines from the reference tests (Figure 10). From the reference tests, the influence of density was clearly seen, *i.e.* the greater the density the greater the maximum deviator stress and the smaller the corresponding strain. Two specimens fell apart during sampling and the results are shown in parentheses as these do not represent the maximum deviator stress for the intact material from the field experiment.

No systematic deviations from the reference results were seen in relation to deviator stress at failure (Figure 10, left). A scatter was seen in the strain at failure, but a reduction of strain at failure was observed for all specimens taken from the innermost positions of block R7, marked with black solid circles, compared to reference tests (Figure 10, right).

The shear strength (Figure 11), determined as the deviator stress at failure on the tall specimens, was plotted with a best-fit line from the reference tests and a broken line representing a model for shear strength, also determined as the deviator stress at failure but based on triaxial tests on bentonite presented by Börgesson *et al.* (1995). The difference between the model and the reference data can be explained by the difference in strain rate, which was lower in the triaxial tests. No systematic deviations from the reference results were seen.

The reduction in strain at failure in the samples from the inner part of the buffer compared to the reference

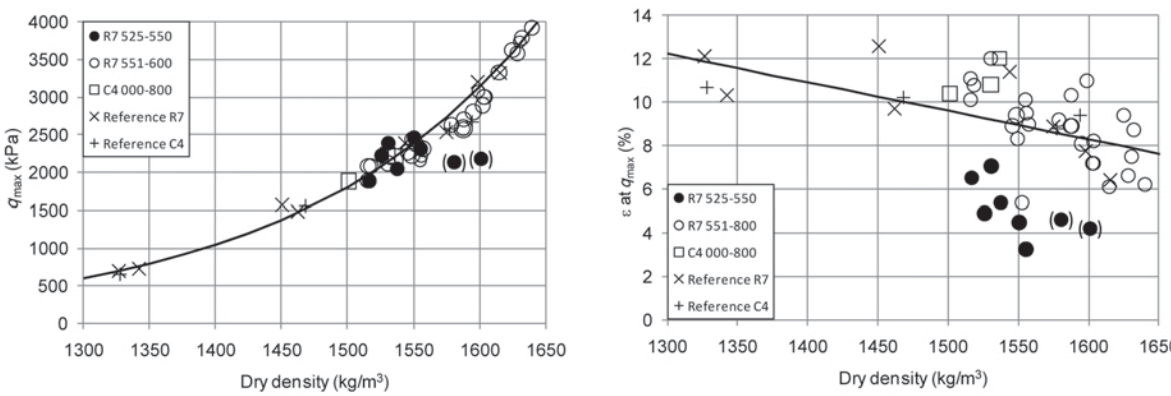

Figure 10. Maximum deviator stress (left) and the corresponding strain (right) *vs*. dry density determined on short specimens.

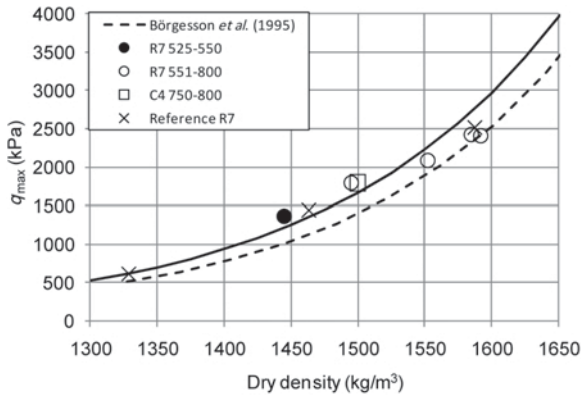

Figure 11. Maximum deviator stress *vs*. dry density determined on tall specimens.

tests, agreed with the results presented by Karnland *et al.* (2009), based on observations of specimens from a field experiment with comparable or higher temperatures. In the present study the reduction in strain at failure occurred at a position where accumulation of calcium sulfate was observed. In the comparable experiment (Karnland *et al.*, 2009), a reduction in strain at failure was observed at positions with increased concentration of calcium sulfate but also at positions where no accumulation of calcium sulfate was seen. In the same study, short-term laboratory heating tests were also performed which also showed a reduction in strain at failure compared to reference tests.

SUMMARY AND CONCLUSIONS

The mineralogical stability of bentonite clays in different geological environments was one of the reasons for choosing bentonite as a buffer material in the Swedish KBS-3 concept for a repository for high-level radioactive waste. Nevertheless, alteration processes are expected to occur under the hydrothermal conditions that will prevail in the bentonite buffer. The present study of MX-80 bentonite subjected to heating at temperatures up to 95ºC and hydration by a natural Na-Ca-Cl type groundwater (~4000 mg Cl^-/L) in a 5 y-long, full-scale heater experiment suggested that:

(1) Under the thermal and hydration gradients that prevailed during the test period, calcium sulfate (anhydrite) accumulated near the canister in the heated part of the buffer.

(2) The major change in the exchangeable cation pool was a loss of Mg in the outer parts of the bentonite blocks at the hydration source, suggesting some replacement of Mg along with the saturation with the Na-Ca-dominated groundwater.

(3) Near the surface of the Cu canister, Cu was incorporated into the bentonite in a non-exchangeable, insoluble form.

(4) The crystal chemistry, the XRD characteristics, and the CEC properties of purified, Na-converted <1 μm fractions provided no evidence of any structural changes in the montmorillonite.

(5) The swelling pressure of the field test material was in the same range as that of the reference material.

(6) The hydraulic conductivity of the trimmed specimens taken from the field experiment was somewhat less than that in tests of the reference material, especially at higher densities.

(7) A reduction in strain at failure was observed on material taken close to the canister in the heated part of the buffer.

(8) No change in deviator stress at failure was seen in field-experiment material.

Whereas no structural alteration of the montmorillonite was detected, dissolution/precipitation and cation exchange reactions along with the water saturation under non-isothermal conditions resulted in small-scale chemical alterations of the bentonite. Small changes were also observed in some of the THM properties of the bentonite retrieved from the field experiment. The exposure to high temperature may, in itself, have affected the mechanical properties of the bentonite, as demonstrated in short-term laboratory heating tests, but the reduction in strain at failure observed at positions close to the canister may be related to anhydrite accumulation at the heater. In contrast, no evidence of coupling was found between the somewhat lower hydraulic conductivity of the trimmed bentonite samples and their positions relative to the heater. Based on this study no indication of significant changes of the performance of the buffer was found.

ACKNOWLEDGMENTS

The authors thank Reiner Dohrmann, Associate Editor of *Clays and Clay Minerals*, and two anonymous reviewers for constructive and valuable comments on the manuscript. The study was financed by the Swedish Nuclear Fuel and Waste Management Company (SKB).

REFERENCES

Ammann, L., Bergaya, F., and Lagaly, G. (2005) Determination of the cation exchange capacity of clays with copper complexes revisited. *Clay Minerals*, **40**, 441–453.

Belyayeva, N.I. (1967) Rapid method for the simultaneous determination of the exchange capacity and content of exchangeable cations in solonetzic soils. *Soviet Soil Science*, 1409–1413.

Birgersson, M. and Karnland, O. (2009) Ion equilibrium between montmorillonite interlayer space and an external solution – consequences for diffusional transport. *Geochimica et Cosmochimica Acta*, **73**, 1908–1923.

Börgesson, L., Johannesson, L.-E., Sandén, T., and Hernelind, J. (1995) Modelling of the physical behaviour of water saturated clay barriers. Laboratory tests, material models and finite element application, SKB Technical Report TR-95-20.

Börgesson, L., Johannesson, L.-E., and Hernelind, J. (2004) Earthquake induced rock shear through a deposition hole. Effect on the canister and the buffer. SKB Technical Report TR-04-02.

Dixon, D.A., Graham, J., and Gray, M.N. (1999) Hydraulic conductivity of clays in confined tests under low hydraulic gradients. *Canadian Geotechnical Journal*, **36**, 815–827.

Dixon, D., Chandler, N., Graham, J., and Gray M.N. (2002) Two large-scale sealing tests conducted at Atomic Energy of Canada's underground research laboratory: the buffer-container experiment and the isothermal test. *Canadian Geotechnical Journal*, **39**, 503–518.

Dohrmann, R. and Kaufhold, S. (2010) Determination of exchangeable calcium of calcareous and gypsiferous bentonites. *Clays and Clay Minerals*, **58**, 79–88.

Dueck, A. (2010) Thermo-mechanical cementation effects in bentonite investigated by unconfined compression tests. SKB Technical Report TR-10-41.

Dueck, A., Börgesson, L., and Johannesson, L.-E. (2010) Stress strain relation of bentonite at undrained shear. Laboratory tests to investigate the influence of material composition and test technique. SKB Technical Report TR-10-32.

Eng, A. (2008) Canister Retrieval Test, Retrieval phase, Project report, SKB International Progress Report IPR-08-13.

ENRESA (2006) FEBEX Full-scale Engineered Barriers Experiment, Updated Final Report 1994–2004. Publicación Técnica ENRESA 05-0/2006, Madrid.

Fernández, A.M. and Villar, M.V. (2010) Geochemical behaviour of a bentonite barrier in the laboratory after up to 8 years of heating and hydration. *Applied Geochemistry*, **25**, 809–824.

Gens, A., Sánchez, M., Guimarães, L. Do N., Alonso, E.E., Lloret, A., Olivella, S., Villar, M.V., and Huertas, F. (2009) A full-scale in situ heating test for high-level nuclear waste disposal: observations, analysis and interpretation. *Géotechnique*, **59**, 377–399.

Gómez-Espina, R. and Villar, M.V. (2010) Geochemical and mineralogical changes in compacted MX-80 bentonite submitted to heat and water gradients. *Applied Clay Science*, **47**, 400–408.

Goudarzi, R. and Börgesson, L. (2006) Canister Retrieval Test, Sensors data report (Period 001026-060501) Report No: 12, SKB International Progress Report IPR-06-35.

Huang, W.-L., Longo, J.M., and Pevear, D.R. (1993) An experimentally derived kinetic model for smectite-to-illite conversion and its use as a geothermometer. *Clays and Clay Minerals*, **41**, 162–177.

Jackson, M.L. (1975) *Soil Chemical Analysis – Advanced Course*, 2nd edition. Madison, Wisconsin, USA.

Johannesson, L.-E. (2007) Canister Retrieval Test, Dismantling and sampling of the buffer and determination of density and water ratio, SKB International Progress Report IPR-07-16.

Karnland, O., Sandén, T., Johannesson, L.-E., Eriksen, T.E., Jansson, M., Wold, S., Pedersen, K., Motamedi, M., and Rosborg, B. (2000) Long term test of buffer material. Final report on the pilot parcels. SKB Technical Report TR-00-22.

Karnland, O. and Birgersson, M. (2006) Montmorillonite stability – with special respect to KBS-3 conditions, SKB Technical Report TR-06-11.

Karnland, O., Olsson, S., and Nilsson, U. (2006) Mineralogy and sealing properties of various bentonites and smectite-rich clay materials. SKB Technical Report TR-06-30.

Karnland, O., Nilsson, U., Weber, H., and Wersin, P. (2008) Sealing ability of Wyoming bentonite pellets foreseen as buffer material – laboratory results. *Physics and Chemistry of the Earth*, **33**, 472–475.

Karnland, O., Olsson, S., Dueck, A., Birgersson, M., Nilsson, U., Hernan-Håkansson, T., Pedersen, K., Nilsson, S., Eriksen, T., and Rosborg, B. (2009) Long term test of buffer material at the Äspö Hard Rock Laboratory, LOT project. Final report on the A2 test parcel. SKB Technical Report TR-09-29.

Meier, L.P. and Kahr, G. (1999) Determination of the cation exchange capacity (CEC) of clay minerals using the complexes of copper(II) ion with triethylenetetramine and tetraethylenepentamine. *Clays and Clay Minerals*, **47**, 386–388.

Kaufhold, S. and Dohrmann, R. (2007) Implications from the LOT experiment regarding the selection of an optimum HLRW bentonite. Clays in Natural and Engineered Barriers for Radioactive Waste Confinement. 3rd International Meeting September 2007, Lille, France, Abstracts, pp. 85–86.

Plötze, M., Kahr, G., Dohrmann, R., and Weber, H. (2007) Hydro-mechanical, geochemical and mineralogical characteristics of the bentonite buffer in a heater experiment: The HE-B project at the Mont Terri Rock Laboratory. *Physics and Chemistry of the Earth*, **32**, 730–740.

SKB (2006) Long-term safety for KBS-3 repositories at Forsmark and Laxemar – a first evaluation. Main Report of the SR-Can project. SKB Technical Report TR-06-09.

Villar, M.V. and Lloret, A. (2007) Dismantling of the first section of the FEBEX *in situ* test: THM laboratory tests on the bentonite blocks retrieved. *Physics and Chemistry of the Earth*, **32**, 716–729.

(*Received 1 April 2011; revised 13 October 2011; Ms. 560; A.E. R. Dohrmann*)